Research Article | Vol. 27, No. 11 | 27 May 2019 | OPTICS EXPRESS 15495
Optics EXPRESS

Enhancement in speed and responsivity of uni-traveling carrier photodiodes with $GaAs_{0.5}Sb_{0.5}/In_{0.53}Ga_{0.47}As$ type-II hybrid absorbers

NASEEM,[1] ZOHAUDDIN AHMAD,[1] RUI-LIN CHAO,[1,2] HSIANG-SZU CHANG,[3] C.-J. NI,[3] H.-S. CHEN,[3] JACK JIA-SHENG HUANG,[3,4] EMIN CHOU,[3] YU-HENG JAN,[3,4] AND JIN-WEI SHI[1,*]

[1]*Department of Electrical Engineering, National Central University, Jungli, 320, Taiwan*
[2]*Department of Photonics, National Chiao-Tung University, Hsinchu, 300, Taiwan*
[3]*Source Photonics, No.46, Park Avenue 2nd Rd., Science-Based Industrial Park, Hsinchu, Taiwan*
[4]*Source Photonics, 8521 Fallbrook Avenue, Suite 200, West Hills, CA 91304, USA*
**jwshi@ee.ncu.edu.tw*

Abstract: We demonstrate a top-illuminated high-speed uni-traveling carrier photodiode (UTC-PD) with a novel design in the p-type absorber, which can effectively shorten the photon absorption depth at telecommunication wavelengths (1.31~1.55 μm) and further enhance the bandwidth-efficiency product of UTC-PD. In our proposed new UTC-PD structure, the p-type $In_{0.53}Ga_{0.47}As$ absorption layer is replaced by the type-II $GaAs_{0.5}Sb_{0.5}$ (p)/$In_{0.53}Ga_{0.47}As$ (i) hybrid absorber. Due to the narrowing of the bandgap and enhancement of the photo-absorption process at the type-II interface between the $GaAs_{0.5}Sb_{0.5}$ and $In_{0.53}Ga_{0.47}As$ layers, our device shows an over 16.7% improvement in the responsivity compared with that of UTC-PD with the same thickness of pure $In_{0.53}Ga_{0.47}As$ absorber (0.7 μm) and a zero optical coupling loss. Our demonstrated device with a simple top-illuminated structure offers a large active mesa (25 μm), a wide optical-to-electrical (O-E) bandwidth (33 GHz), a high responsivity (0.7 A/W), and a high saturation current (>5 mA) under 1.31 μm optical wavelength. These promising results suggest that our proposed PD structure can fundamentally overcome the trade-off among bandwidth, efficiency, and device active diameter of high-speed PDs.

1. Introduction

The progress of data rate per channel in the optical interconnect (OI) system drives the increase of required bandwidth for both transmitter and receiver. In the newly developed 400 Gbit/sec Ethernet system with 4 fiber channels, the corresponding data rate per channel is 112 Gbit/sec. In order to attain such high data rate, one of the possible solutions is utilizing the pulse-amplitude modulation-4 (PAM-4) format with a 56 Gbaud per channel. A high-responsivity p-i-n photodiode operated at 1.31 μm wavelength with a 3-dB optical-to-electrical (O-E) bandwidth over 30 GHz and a large aperture size, serves as the key component in the receiving-end of the aforementioned Ethernet system. Commercially available 10 Gbit/sec InP based PD chips at 1.31-1.55 μm wavelength typically have around 50 μm active diameters, providing the sufficient alignment tolerance for ROSA package. However, when the required bandwidth of PD increases, a decrease of the p-i-n PD's active diameter and a reduction of absorption layer thickness are both necessary in order to balance the trade-off between RC-limited and carrier transient time limited bandwidths [1–3]. This leads to penalties of smaller responsivity, larger coupling loss and/or tighter alignment tolerances, and higher packaging costs in ROSA module.

#360571 https://doi.org/10.1364/OE.27.015495
Journal © 2019 Received 19 Feb 2019; revised 20 Mar 2019; accepted 16 Apr 2019; published 15 May 2019

Optics EXPRESS

By use of the waveguide [1,4–6] or edge-coupled PD structures [7], the trade-off between bandwidth and efficiency (responsivity) in high-speed PD can be overcome. In the waveguide PD structure (WGPD) with a thin absorption layer thickness, the high-efficiency performance can be sustained by properly increasing the device absorption length. Furthermore, the thin absorber can also lead to a wide internal carrier transient time limited bandwidth. WGPD [1,4–6] and refracting-facet PD [7] with bandwidth-efficiency product as high as 50 GHz have been previously demonstrated. Those WGPD devices exhibited 3-dB O-E bandwidth (BW) of 50 GHz and quantum efficiency (QE) of 80% or BW of 110 GHz and QE of 50%. However, the WGPD structure usually has a much smaller alignment tolerance and higher fabrication cost, compared to the top-illuminated PD structure. To fundamentally overcome the trade-offs among bandwidth, efficiency, and coupling alignment of PD, adopting the photo-absorption layer with an absorption coefficient larger than that of the bulk $In_{0.53}Ga_{0.47}As$ material [2,3], appears to be one of the most effective approaches over the WGPD design. The increase of photo-absorption coefficient leads to the decrease in the required absorption layer thickness for the desired responsivity performance and the enhancement of carrier transient time limited bandwidth.

In our previous studies [2,3], we have demonstrated that the InP/$In_{0.53}Ga_{0.47}As$-based PDs can achieve superior performance, including higher bandwidth-efficiency product and the enlarged device active area, compared to those of the GaAs-based ones for 850 nm wavelength. The performance advantage of $In_{0.53}Ga_{0.47}As$-based PD is attributed to the larger absorption coefficient of the $In_{0.53}Ga_{0.47}As$ layer with respect to the GaAs (~3 vs. ~0.8 μm^{-1}) at such wavelength. On the other hand, for the operations at telecommunication wavelengths (1.31-1.55 μm), in order to have the photo-absorption layer, such as $In_{0.8}Ga_{0.2}As$, with a narrower bandgap (0.5 vs. 0.75 eV) than that of bulk $In_{0.53}Ga_{0.47}As$ material, the thick lattice-mismatched buffer layer grown on the InP substrate is necessary [8,9]. However, this leads to increased dark current and reliability issues of fabricated PDs. In this paper, we demonstrate a top-illuminated high-speed uni-traveling carrier photodiode (UTC-PD) with a novel design in the lattice-matched p-type absorber with InP substrate, which can effectively shorten the photon absorption depth at 1.31~1.55 μm wavelength and further enhance the bandwidth-efficiency product of UTC-PD. In our proposed new UTC-PD structure, the p-type $In_{0.53}Ga_{0.47}As$ absorption layer is replaced by the type-II $GaAs_{0.5}Sb_{0.5}$ (p)/$In_{0.53}Ga_{0.47}As$ (i) hybrid absorber. Owing to the narrowing of the bandgap and enhancement of the photo-absorption process at the type-II interface between the $GaAs_{0.5}Sb_{0.5}$ and $In_{0.53}Ga_{0.47}As$ layers [10,11], our device shows an over 16.7% improvement in the responsivity as compared to that of UTC-PD with the pure $In_{0.53}Ga_{0.47}As$ absorber and the same total thickness (0.7 μm). Furthermore, our demonstrated device with a simple top-illuminated structure can offer a large active mesa (25 μm), a wide optical-to-electrical (O-E) bandwidth (33 GHz), a high responsivity (0.7 A/W), and a high saturation current (> 5 mA) under 1.31 μm optical wavelength. These excellent performances are comparable with those of high-performance 56 Gbaud PD [12] with the same top-illuminated structure and a smaller mesa size (~16 μm). This suggests that our proposed PD structure can fundamentally overcome the trade-off among bandwidth, efficiency, and device active diameter of high-speed PDs.

2. Design of device structure and fabrication

Figure 1(a) shows the simulated band diagram of our demonstrated device structure. Our epilayer structure was grown on the semi-insulating (S.I.) InP substrate in a molecular-beam epitaxy (MBE) chamber [13]. From top to bottom, it is composed of the p^+-$In_{0.53}Ga_{0.47}As$ contact layer, p^+-$Al_{0.3}Ga_{0.7}As_{0.5}Sb_{0.5}$ electron blocking layer, p-type hybrid absorber, InP collector layer, and n^+ InP contact layer. The detailed material composition, thickness, and doping density of each layer are given in Table 1. Here, the hybrid absorption region with a type-II band alignment ($GaAs_{0.5}Sb_{0.5}$/$In_{0.53}Ga_{0.47}As$) is comprised of two major parts. The first is the p-type $GaSb_{0.5}As_{0.5}$ absorption layer with a thickness of 300 nm and a graded doping

Optics EXPRESS

profile (top: 1×10^{19} cm^{-3} to bottom: 5×10^{16} cm^{-3}) designed to induce built-in electric (E-) field and accelerate the electron diffusion process. As shown in Fig. 1(a), we can clearly see that there is a small built-in E-field in this $GaAs_{0.5}Sb_{0.5}$ absorption layer due to the graded doping profile. The second is an intrinsic $In_{0.53}Ga_{0.47}As$ layer with a thickness of 400 nm. As compared to the device structure reported in our previous work [11], which is targeted on THz O-E bandwidth, the thickness of type-II hybrid absorption layer in this work is greatly increased from 160 to 700 nm in order to enhance the responsivity performance for around 30 GHz O-E bandwidth. The un-doped $In_{0.53}Ga_{0.47}As$ layer is inserted in the p-type absorption region of the traditional UTC-PD to minimize the electron recombination process. Although such an intrinsic layer may contribute to undesired hole transport, the corresponding transient time limited bandwidth of the holes is still as high as around 55 GHz, larger than the measured net O-E bandwidth of our device (around 33 GHz), which will be discussed in greater detail later. As shown in Fig. 1(a), the type-II band alignment between the interface of the $GaAs_{0.5}Sb_{0.5}$ and $In_{0.53}Ga_{0.47}As$ layers reduces the effective bandgap to 0.5 eV (~2.4 μm cut-off wavelength [10]), which can further enhance the absorption process under 1.3 to 1.55 μm wavelengths excitation. Our collector layer consists of an intrinsic InP layer with an ultra-low background doping density in order to reduce the required bias voltage for the full depletion in collector layer. In addition, its thickness (1.2 μm) is optimized to balance the RC-limited and internal transient time limited bandwidths for a 30 μm diameter of active mesa. Figure 1(b) shows the picture of top-view of demonstrated PD. The fabricated device has a typical top-illuminated structure with a 25 μm diameter of active mesa and is integrated with a coplanar ground-signal (GS) pads for on-wafer high-speed measurement. An anti-reflection coating film, which is composed of Si_3N_4 with an around 200 nm thickness, is deposited on top of our device to minimize the reflection loss of the launched optical signal at 1.31 or 1.55 μm wavelength.

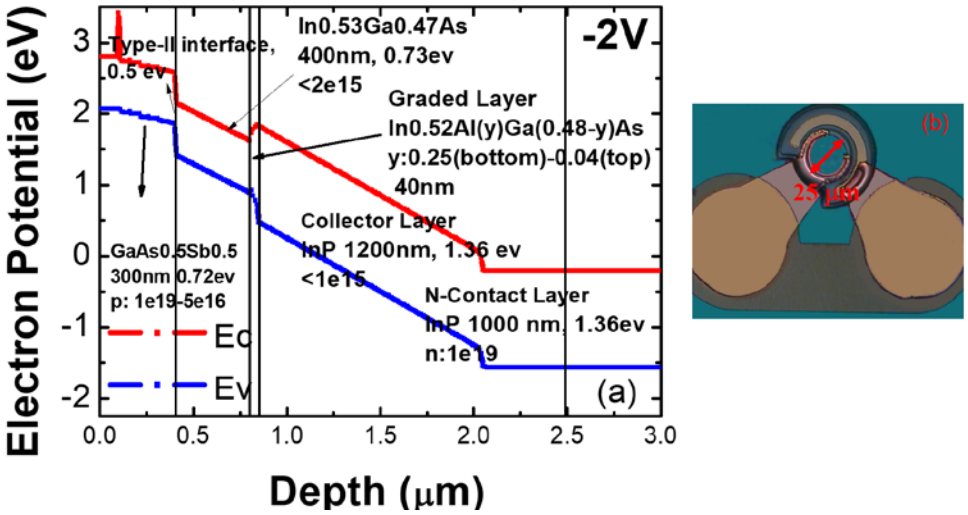

Fig. 1. (a). Simulated band diagram of the demonstrated hybrid-absorber UTC-PDs under –2 V bias voltage. The unit for doping density in each layer is cm^{-3}. (b) Photo of top-view of the fabricated devices.

3. Measurement results

Here our PDs of Device-A and Device-B were fabricated with the active diameters of 25 and 30 μm, respectively. The corresponding aperture size of optical window is 15 and 20 μm, respectively. The measured dark currents of device A and B under –5 V bias is in the range of

Optics EXPRESS

90-110 nA. Under –2V bias, the measured DC responsivity of our demonstrated PD at 1.31 and 1.55 μm wavelength is around 0.7 and 0.53 A/W, respectively. The reported absorption coefficients of bulk $GaAs_{0.5}Sb_{0.5}$ layers (lattice-matched on InP substrate) at 1.31 and 1.55 μm wavelength are 0.9 and 0.68 μm^{-1}, respectively [14]. They are comparable with those of bulk $In_{0.53}Ga_{0.47}As$ layer (1.2 and 0.68 μm^{-1} at 1.31 and 1.55 μm wavelength, respectively) [14]. Based on these reported absorption coefficients and the assumption of single-pass optical path in the absorber, the theoretical maximum responsivity is 0.56 (0.47) A/W for our device with a zero optical coupling/reflection loss and a 0.7 μm absorption layer thickness at the 1.31(1.55) μm wavelength. The validness of single-pass assumption is due to that the reflected optical beam from substrate side is far from the absorption region, which would suffer significant diffraction loss and can't contribute to the photocurrent. Such measurement result clearly indicates that the type-II interface in our hybrid absorber can contribute to around 26 and 12% enhancements in the DC responsivity under 1.31 and 1.55 μm wavelength excitations, respectively, due to its narrower bandgap in the type-II interface as discussed. Furthermore, as compared to the PD with a pure $In_{0.53}Ga_{0.47}As$ absorber and the same total thickness (0.7 μm), our device can still have >16.7% enhancement in responsivity under the 1.31 μm wavelength excitation and zero optical coupling loss. Figures 2 and 3 show the measured bias-dependent O-E frequency responses of Device-A and -B under low (0.1 mA) and high (1 mA) output photocurrents at 1.31 μm wavelength, respectively. We can clearly see that when the reverse bias is over –2 V, the measured 3-dB O-E bandwidths of Device-A and -B are around 33 and 28 GHz, respectively. Furthermore, regardless of high or low output current, the measured 3-dB O-E bandwidths of both devices remain unchanged. This measurement result clearly indicates the good linearity of our device, which is a critical issue in the performance of PAM-4 receiver [15].

Table 1. Epitaxy structures of demonstrated devices

	PIN-PD			
	Material	**Thickness (Å)**	**Doping Level (/cm^3)**	**Type**
P-Contact layer	**$In_{0.53}Ga_{0.47}As$**	**1000**	**3.0E + 19**	**P^+**
Electron block layer	**$Al_{0.3}Ga_{0.7}As_{0.5}Sb_{0.5}$**	**100**	**1.0E + 19**	**P^+**
P-absorber layer	**$GaAs_{0.5}Sb_{0.5}$**	**3000**	**1E + 19 (top) to 5E + 16 (bottom)**	**P**
i-absorber layer	**$In_{0.53}Ga_{0.47}As$**	**4000**	**<2E + 15**	
i-graded bandgap layer	**$In_{0.53}Ga_{0.47}As/In_{0.52}Al_{0.48}As$ Super-lattice**	**400**		
i-collector layer	**InP**	**12000**	**<1.0E + 15**	
N-contact layer	**InP**	**10000**	**>1.0E + 19**	**N^+**
Buffer layer	**InP**	**1000**		
Semi-insulating InP Substrate	**InP**			

3. Measurement results

Here our PDs of Device-A and Device-B were fabricated with the active diameters of 25 and 30 μm, respectively. The corresponding aperture size of optical window is 15 and 20 μm, respectively. The measured dark currents of device A and B under –5 V bias is in the range of 90-110 nA. Under –2V bias, the measured DC responsivity of our demonstrated PD at 1.31 and 1.55 μm wavelength is around 0.7 and 0.53 A/W, respectively. The reported absorption coefficients of bulk $GaAs_{0.5}Sb_{0.5}$ layers (lattice-matched on InP substrate) at 1.31 and 1.55 μm wavelength are 0.9 and 0.68 μm^{-1}, respectively [14]. They are comparable with those of bulk

Optics EXPRESS

$In_{0.53}Ga_{0.47}As$ layer (1.2 and 0.68 μm^{-1} at 1.31 and 1.55 μm wavelength, respectively) [14]. Based on these reported absorption coefficients and the assumption of single-pass optical path in the absorber, the theoretical maximum responsivity is 0.56 (0.47) A/W for our device with a zero optical coupling/reflection loss and a 0.7 μm absorption layer thickness at the 1.31(1.55) μm wavelength. The validness of single-pass assumption is due to that the reflected optical beam from substrate side is far from the absorption region, which would suffer significant diffraction loss and can't contribute to the photocurrent. Such measurement result clearly indicates that the type-II interface in our hybrid absorber can contribute to around 26 and 12% enhancements in the DC responsivity under 1.31 and 1.55 μm wavelength excitations, respectively, due to its narrower bandgap in the type-II interface as discussed. Furthermore, as compared to the PD with a pure $In_{0.53}Ga_{0.47}As$ absorber and the same total thickness (0.7 μm), our device can still have >16.7% enhancement in responsivity under the 1.31 μm wavelength excitation and zero optical coupling loss. Figures 2 and 3 show the measured bias-dependent O-E frequency responses of Device-A and -B under low (0.1 mA) and high (1 mA) output photocurrents at 1.31 μm wavelength, respectively. We can clearly see that when the reverse bias is over –2 V, the measured 3-dB O-E bandwidths of Device-A and -B are around 33 and 28 GHz, respectively. Furthermore, regardless of high or low output current, the measured 3-dB O-E bandwidths of both devices remain unchanged. This measurement result clearly indicates the good linearity of our device, which is a critical issue in the performance of PAM-4 receiver [15].

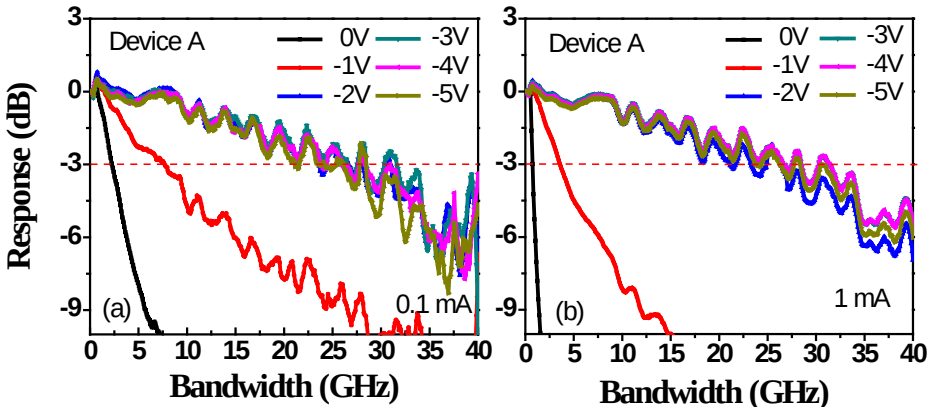

Fig. 2. Bias dependent O-E frequency responses measured under different output photocurrents: (a) 0.1 mA and (b) 1 mA for Device A with a 25 μm active diameter.

Optics EXPRESS

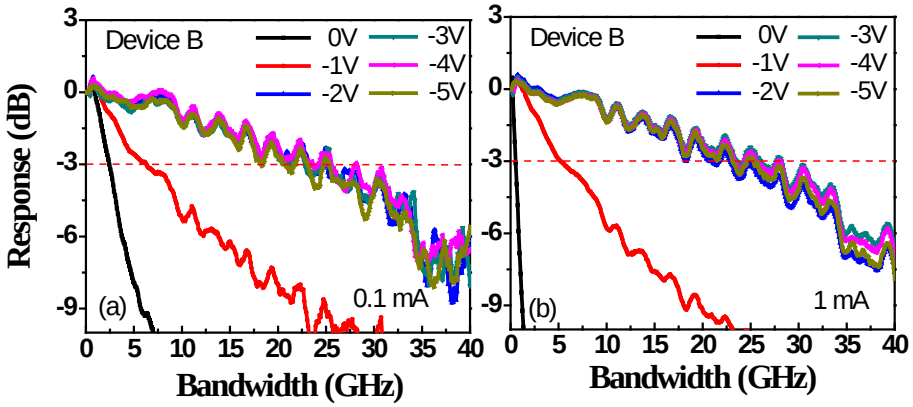

Fig. 3. Bias dependent O-E frequency responses measured under different output photocurrents: (a) 0.1 mA and (b) 1 mA for Device B with a 30 μm active diameter.

The overall O-E 3-dB bandwidth (f_{3dB}) of a PD is determined by the carrier transport time $\left(1/f_t\right)$ and the RC time constant $\left(1/f_{RC}\right)$. In order to investigate the internal carrier transport time inside our device, the following equation has been adopted [1,2].

$$\frac{1}{f_{3dB}^2}=\frac{1}{f_{RC}^2}+\frac{1}{f_t^2}=\left(2\pi RC\right)^2+\frac{1}{f_t^2} \tag{1}$$

Where R is the sum of the parasitic resistance and the load resistance (50 Ω) and C is the total capacitance. Here, the RC-limited bandwidth can be extracted by use of the measured scattering parameters of microwave reflection coefficients (S_{22}) [2]. Figure 4 shows the adopted equivalent circuit models for fitting of S_{22} parameters of devices A and B. The fitted values of each circuit elements of devices A and B are shown in the Table 2. During our device modeling process for the extraction of extrinsic f_{RC} of PD chips, the two artificial circuit elements; R_T and C_T, have been removed. This is because that they are used to mimic the low-pass frequency response of internal carrier transient time [16,17]. Figure 5(a) and (b) shows the fitted and measured frequency responses of S_{22} parameters on Smith Chart of Device- A and B, respectively. Clearly, there is a good match between the simulated and measured results from 40 MHz to 40 GHz. By use of the extracted equivalent circuit model and choose the proper values of R_T and C_T, as shown in Table 2, to fit the measured O-E frequency response, we can then determine the internal transient time limited frequency responses of our device.

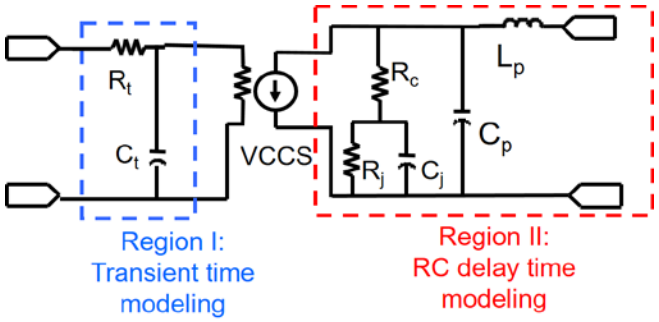

Fig. 4. Equivalent-circuit-model. VCCS: voltage controlled current source.

Optics EXPRESS

Table 2. Values of the circuit elements

	Physical Meaning	Device A	Device B
C_j	Junction Capacitance (fF)	36	53
R_j	Junction Resistance (kΩ)	90	90
R_C	Contact Resistance (Ω)	10	11
C_p	Parasitic Capacitance (fF)	30	47
L_p	Parasitic Inductance (pH)	11	11
R_t	Artificial Resistance (Ω)	26	11
C_t	Artificial Capacitance (fF)	41	22

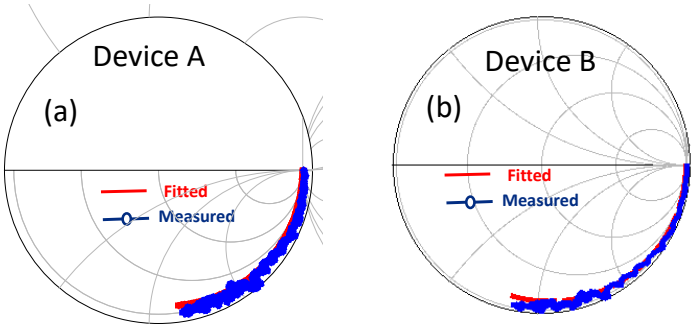

Fig. 5. Measured (blue line) and fitted (red line) S_{22} parameters from near dc to 40 GHz under a fixed dc bias (–2 V) for (a) Device-A and (b) Device-B.

Figure 6(a) and (b) shows the RC-limited, measured O-E, fitted O-E, and transient time limited frequency responses of Device-A and -B, respectively. We note that Device-B exhibited the RC-limited bandwidth is close to the transient-time-limited value of around 35 GHz. This indicates that our collector layer thickness has been optimized to balance the f_t and f_{RC}. The other way to extract the internal carrier transient time is based on Eq. (1) as discussed. Figure 6(c) shows the $\left(1/f_{RC}\right)^2$ vs. $\left(10^3/f_{3dB}^2\right)$ values for Devices A and B. With Eq. (1), the internal carrier transient time in our device is determined using the intercepts shown along the y-axis of this Fig [1,2]. The obtained f_t is around 33.5 GHz. Such number is consistent with the transient time limited bandwidth (around 35 GHz) obtained by the equivalent circuit modeling technique, as shown in Figs. 6(a) and (b). The drift-diffusion model is used to estimate the transient time and corresponding electron/hole drift-velocity across each layers [18]. The extracted electron drift-velocity through the 1.2 μm InP collector layer is around 11×10^5 m/sec. The dominating factor for the total transient time inside our proposed epi-layer structure should be the drift-time of the photo-generated holes through the depleted 400 nm thick $In_{0.53}Ga_{0.47}As$ absorption layer. The average drift-velocity of electrons and holes across this layer is around 5×10^4 m/sec, which is close to the value reported (5.3×10^4 m/sec) for $In_{0.53}Ga_{0.47}As$ p-i-n PDs [1]. The electron minority mobility in the p-type $GaAs_{0.5}Sb_{0.5}$ layer with a graded doping profile is 4000 cm^2/V-sec. This number is pretty close to that in the p-type $In_{0.53}Ga_{0.47}As$ absorption layer of UTC-PD (~5000 cm^2/V-sec) [19], which indicates the good material quality of our thick (300 nm) $GaAs_{0.5}Sb_{0.5}$ layer.

Optics EXPRESS

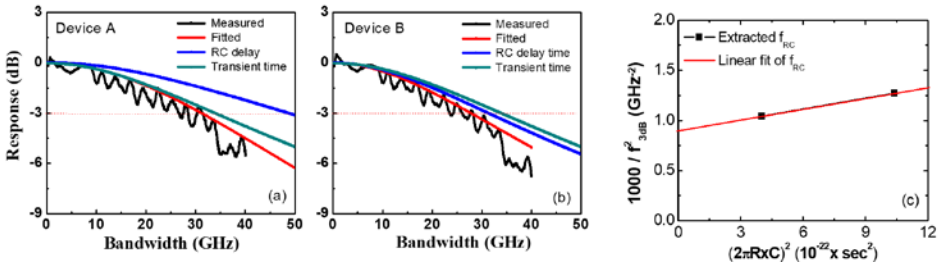

Fig. 6. The measured O-E, extracted RC-limited, transient time, and fitted O-E frequency responses of devices (a) A and (b) B. (c) The extracted $\left(1/f_{RC}\right)^2$ versus the measured $\left(10^3/f_{3dB}^2\right)$ for devices A and B.

The PDs with high-linearity performance is required for PAM-4 modulation format. The two-laser heterodyne-beating setup at 1.55 μm wavelengths is used to test the output saturation current of our demonstrated PD [5]. Figure 7(a) and (b) shows the measured photo-generated microwave power versus output photocurrent for Device-A and -B obtained under different reverse biases (–2 to –5V). The measurement frequency chosen was around the 3-dB O-E bandwidth at 30 GHz. The ideal relation between the microwave power and averaged photocurrent (solid line) with a 100% optical modulation depth under a 50 Ω load is also plotted for reference. We can clearly see that the saturation currents of Device-A and -B under –5 V bias are around 5 and 13 mA, respectively. Such high output current can far exceed the required overload optical power (+ 4.5 dBm; around 2 mA photocurrent) for the 400 Gbit/sec receiver with PAM-4 modulation format. Based on the aforementioned dynamic and static measurements results, our demonstrated PD (Device A) with a larger active mesa (25 vs. 16 μm) can achieve a comparable 3-dB O-E bandwidth (~33 vs. 38 GHz), responsivity (0.7 vs. 0.8 A/W), and a higher saturation current as compared to those of high-performance and commercial available p-i-n PD with the same top-illuminated structure for 56 Gbaud application [12].

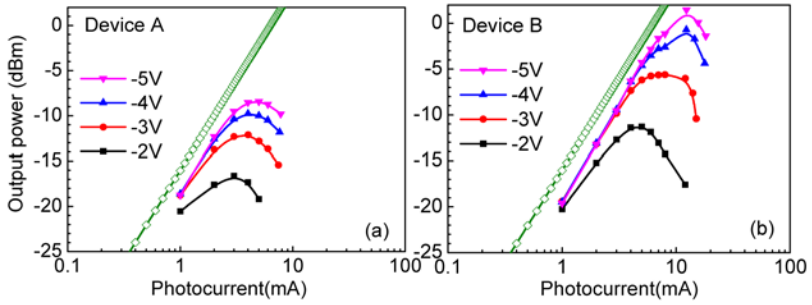

Fig. 7. The measured photo-generated microwave power versus photocurrent for device (a) A and (b) B under sinusoidal signal excitation and with different reverse biases at operating frequencies of 30 GHz. The open symbol line shows the ideal trace for a 100% optical modulation depth and 50 Ω load.

4. Conclusion

In conclusion, we demonstrate the UTC-PD structure with a novel design in its hybrid absorber. Using the narrow bandgap (~0.5 eV) of the type-II interface between p-type $GaAs_{0.5}Sb_{0.5}$ and intrinsic $In_{0.53}Ga_{0.47}As$ absorbers, we can achieve an enhanced responsivity

Optics EXPRESS

by over 16.7% (at 1.31 μm wavelength) as compared to that of the PD based on a pure $In_{0.53}Ga_{0.47}As$ absorber with the same total thickness (700 nm) of absorption region, and a zero optical coupling loss. Our demonstrated device with a simple top-illuminated structure and a large active mesa (25 μm) can provide a wide optical-to-electrical (O-E) bandwidth as 33 GHz, high responsivity (0.7 A/W), and a high saturation current (>5 mA) under 1.31 μm optical wavelength. These promising results suggest that our proposed hybrid absorber structure can fundamentally overcome the trade-off among bandwidth, efficiency, and device active diameter of high-speed PDs due to its stronger photo-absorption process at telecommunication wavelengths (1.3 to 1.55 μm) than that of bulk $In_{0.53}Ga_{0.47}As$ layer. In our future work, we will experiment with the packaging of such novel PDs with high-performance trans-impedance amplifiers to study the sensitivity performance for 56 Gbaud applications.

Funding

Ministry of Science and Technology in Taiwan (107-2622-E-008 –002 -CC2 and 106-2221-E-008 –063 -MY3).

References

1. K. Kato, “Ultrawide-band/high-frequency photodetectors,” IEEE Trans. Microw. Theory Tech. **47**(7), 1265–1281 (1999).
2. J.-W. Shi, K.-L. Chi, C.-Y. Li, and J.-M. Wun, “Dynamic analysis of high-efficiency InP based photodiode for 40 Gbit/sec optical interconnect across a wide optical window (0.85 to 1.55 μm),” IEEE/OSA J. Lightwave Technol. **33**(4), 921–927 (2015).
3. J.-W. Shi, C.-Y. Li, K.-L. Chi, J.-M. Wun, Y.-M. Hsin, and S. D. Benjamin, “Large-area p-i-n photodiode with high-speed and high-efficiency across a wide optical operation window (0.85 to 1.55 μm),” IEEE J. Sel. Top. Quantum Electron. **20**(6), 3800807 (2014).
4. S. Demiguel, N. Li, X. Li, X. Zheng, J. Kim, J. C. Campbell, H. Lu, and A. Anselm, “Very high-responsivity evanescently coupled photodiodes integrating a short planar multimode waveguide for high-speed applications,” IEEE Photonics Technol. Lett. **15**(12), 1761–1763 (2003).
5. J.-W. Shi, C.-Y. Wu, Y.-S. Wu, P.-H. Chiu, and C.-C. Hong, “High-speed, high-responsivity, and high-power performance of near-ballistic uni-traveling-carrier photodiode at 1.55μm wavelength,” IEEE Photonics Technol. Lett. **17**(9), 1929–1931 (2005).
6. X. Xie, Q. Zhou, E. Norberg, M. Jacob-Mitos, Y. Chen, Z. Yang, A. Ramaswamy, G. Fish, J. C. Campbell, and A. Beling, “High-power and high-speed heterogeneously integrated waveguide-coupled photodiodes on silicon-on-insulator,” IEEE/OSA J. Lightwave Technol. **34**(1), 73–78 (2016).
7. Y. Muramoto, H. Fukano, and T. Furuta, “A polarization-independent refracting-facet uni-traveling-carrier photodiode with high efficiency and large bandwidth,” IEEE/OSA J. Lightwave Technol. **24**(10), 3830–3834 (2006).
8. A. Joshi and S. Datta, “High-speed, large-area, p-i-n InGaAs photodiode linear array at 2-micron wavelength,” Proc. SPIE **8353**, 83533D (2012).
9. N. Ye, H. Yang, M. Gleeson, N. Pavarelli, H. Zhang, J. O’Callaghan, W. Han, N. Nudds, S. Collins, A. Gocalinska, E. Pelucchi, “InGaAs surface normal photodiode for 2 μm optical communication systems,” IEEE Photonics Technol. Lett. **27**(14), 1469–1472 (2015).
10. R. Sidhu, L. Zhang, N. Tan, N. Duan, J. C. Campbell, A. L. Holmes, D.-F. Hsu, and M. A. Itzler, “2.4 μm cutoff wavelength avalanche photodiode on InP substrate,” Electron. Lett. **42**(3), 181–182 (2006).
11. J.-M. Wun, Y.-W. Wang, and J.-W. Shi, “Ultra-fast uni-traveling carrier photodiodes with $GaAs_{0.5}Sb_{0.5}/In_{0.53}Ga_{0.47}As$ type-II hybrid absorbers for high-power operation at THz frequencies,” IEEE J. Sel. Top. Quantum Electron. **24**(2), 8500207 (2018).
12. Albis Optoelectronics AG, “PD40C1: 56 Gbaud Photodiode with Enhanced Responsivity,” http://www.albisopto.com/albis_product/pd40c1-56-gbaud-photodiode-with-enhanced-responsivity/.
13. Intelligent Epitaxy Technology, Inc., “IntelliEPI,” http://intelliepi.com.
14. M. S. Park and J. H. Jang, “$GaAs_{0.5}Sb_{0.5}$ lattice matched to InP for 1.55 μm photo-detection,” Electron. Lett. **44**(8), 549–551 (2008).
15. M. Nada, Y. Muramoto, H. Yokoyama, and H. Matsuzaki, “High-speed high-power-tolerant avalanche photodiode for 100-Gb/s applications,” in Proceedings of IEEE Photonic Society Meeting (IEEE, 2014) pp. 172–173.
16. G. Wang, T. Tokumitsu, I. Hanawa, Y. Yoneda, K. Sato, and M. Kobayashi, “A time-delay equivalent-circuit model of ultrafast p-i-n photodiodes,” IEEE Trans. Microw. Theory Tech. **51**(4), 1227–1233 (2003).
17. Y.-S. Wu, J.-W. Shi, and P.-H. Chiu, “Analytical modeling of a high-performance near-ballistic uni-traveling-carrier photodiode at a 1.55μm wavelength,” IEEE Photonics Technol. Lett. **18**(8), 938–940 (2006).

Optics EXPRESS

18. J.-W. Shi, C.-W. Liu, and C.-W. Liu, "Design and analysis of separate-absorption-transport-charge-multiplication traveling-wave avalanche photodetectors," IEEE/OSA J. Lightwave Technol. **22**(6), 1583–1590 (2004).
19. N. Shimizu, N. Watanabe, T. Furuta, and T. Ishibashi, "InP-InGaAs uni-traveling-carrier photodiode with improved 3-dB bandwidth of over 150GHz," IEEE Photonics Technol. Lett. **10**(3), 412–414 (1998).